Community composition predicts photogrammetry-based structural complexity on coral reefs

J. Carlot, A. Rovère, E. Casella, D. Harris, C. Grellet-Muñoz, Y. Chancerelle, E. Dormy, L. Hédouin, V. Parravicini

Community composition predicts photogrammetry-based structural complexity on coral reefs

J. Carlot[1-2*], A. Rovère[3-4], E. Casella[3-4], D. Harris[5], C. Grellet-Muñoz[1-3], Y. Chancerelle[1-2], E. Dormy [6], L. Hedouin[1-2], V. Parravicini[1-2]

[1]PSL Université Paris: EPHE-UPVD-CNRS, USR 3278 CRIOBE, BP 1013, 98729 Papetoai, Moorea, French Polynesia

[2]Laboratoire d'Excellence « CORAIL »

[3]Centre for Marine Environmental Sciences (MARUM), Bremen University, Bremen, Germany.

[4]Leibniz Centre for Tropical Marine Research, Bremen, Germany.

[5]The University of Queensland, School of Earth and Environmental Sciences, Brisbane, Queensland, Australia.

[6]Department of Mathematics and Applications, CNRS UMR 8553, Ecole Normale Supérieure, Paris, France

Keywords

Coral Complexity – Rugosity measures – Photogrammetry – Reef ecology – Modeling

*Corresponding author: Jérémy Carlot,
PSL Research University
EPHE-UPVD-CNRS
USR 3278 CRIOBE
BP 1013, 98729 Papetoai, Moorea, French Polynesia
Laboratoire d'Excellence « CORAIL »
E-mail: Jeremy.carlot@hotmail.fr

Abstract

The capacity of coral reefs to provide ecosystem services, to keep their diversity and their productivity are related to their three-dimensional structural complexity. This parameter is also correlated to total fish biomass, to the general reef resilience to external stresses and to their ability to dissipate wave energy. However, information on structural complexity (also defined as reef rugosity) has been uncommonly assessed in historical monitoring programs, with the result that the long-term trend of this variable is generally unavailable. In this study, we show that it is possible to predict and hindcast the three-dimensional complexity of coral reefs by combining photogrammetry, statistical modeling and historical benthic community data. We calibrated a lasso generalized linear model to predict structural complexity obtained by 57 photogrammetry transects recorded at 13 sites around the island of Moorea (French Polynesia). Our model was able to predict structural complexity with high accuracy (cross-validated $R^2 = 0.81 \pm 0.12$). We then used our model to hindcast historical trends in 3D structural complexity using community composition data collected in Moorea from 2004 to 2017. The temporal analysis highlighted the dramatic effect of a crown-of-thorns outbreak in 2006-2009 and Cyclone Oli in 2010. These two events together reduce coral cover from ≈50% to almost zero. Our model captured these effects, confirming the possibility to predict structural complexity on the basis of assemblage composition.

Introduction

Global concerns are emerging about the increasing frequency of mass mortality of corals associated to coral bleaching events (Van Oppen and Lough 2009; Heron et al. 2016; Hughes et al. 2017). These disturbances are associated to severe habitat destruction that reduces the structural complexity (i.e., flattening) of coral reefs (Newman et al. 2015). Structural complexity is the three-dimensional spatial arrangement of an ecosystem (McCormick 1994; Chazdon 2014), which is largely due to the growth form and distribution of hard coral. According to the habitat heterogeneity hypothesis (MacArthur and Wilson 1967), the more complex the structure of an ecosystem, the greater the diversity and abundance of associated organisms. On coral reefs, the 3D structural complexity of the habitat is correlated to the biomass and diversity of fish (Willis and Anderson 2003; Gratwicke and Speight 2005; Alvarez-Filip et al. 2009; Rogers et al. 2014), to the reef capacity to recover from disturbance (Graham et al. 2015), but also to the reef ability to dissipate wave energy, thus protecting the shoreline from extreme inundations (Harris et al. 2018). Broad-scale declines in the complexity of coral reefs have been observed both in the Caribbean and the Pacific as a result of both human impacts and climate changes (Hoegh-Guldberg 1999; Hughes et al. 2003; Hoegh-Guldberg et al. 2007; Perry et al. 2018). Despite the well-known important relationship between structural complexity, ecological diversity, abundance and biomass, information on structural complexity is sparse in monitoring programs with the result that long-term trends for this variable are virtually unknown (Graham et al. 2015).

Methods to measure structural complexity (often referred as rugosity, in particular in older literature) on coral reefs first arose in the 70' in articles by Risk (1972) and Hobson (1972). These authors defined three criteria for measuring complexity: 1) the measure had to be easily understandable, 2) it had to be measurable during the fieldwork and, 3) it should be comparable. In early studies, it was proposed that rugosity could be recorded by draping a steel chain over the reef surface, and then measuring the ratio between the total length of the chain

and the planar distance between the ends of the chain. The higher the ratio, the more complex the substratum (Hill and Wilkinson 2004; Graham and Nash 2013). Despite the ease of use of such metric, laying a chain represents a bi-dimensional measure which does not capture the full complexity of complex three-dimensional (3D) habitats such as coral reefs. Although some time-consuming 3D metrics have been proposed in the past (e.g. Parravicini et al. 2006), the recent progress in underwater photogrammetry are finally affording researchers the opportunity to capture the three-dimensionality of coral reefs. For example, Friedman et al. (2012) started to use a georeferenced survey work and each includes a downward-looking camera pair with a baseline of approximately 7cm, pixel resolution of 1360 × 1024 to define rugosity. Others authors like Burns et al. (2015) were using these new advances for defining the rugosity about a transect and extract a complexity index at the species level for 6 species. Leon et al. (2015), defined three roughness parameters, namely the root means square height, tortuosity (i.e. rugosity) and fractal dimension, and were derived and compared in order to asses which one better characterizes reef flat roughness. Naughton et al. (2015) succeed with an accuracy never equaled to define maps of community structures between taxa. Some writers have even pushed the boundaries to measure the small-scale three-dimensional features of a shallow-water coral reef thanks to drone (Casella et al. 2017). Thus, a plethora of works have emerged asking several authors about the chain-tape future (Storlazzi et al. 2016). However, whatever the metric employed (chain-tape or photogrammetry methods), there is still no clear evidence concerning what is driving structural complexity. Some authors claim that it is driven by the presence of some branching species like the Acropora spp. and thus the overall coral cover would not matter (Aronson and Precht 2006; Alvarez-Filip et al. 2009, 2011). Others have found that coral cover is significantly and highly correlated to the rugosity (Halford et al. 2004; Graham and Nash 2013) or species composition (Richardson et al. 2017). But in both cases, there is a common consensus for admitting coral drives complexity which could be used for rebuilding past rugosities.

In this study, we combined statistical modeling to 3D reef transects reconstructed using photogrammetry in order to test the potential to predict coral reef structural complexity on the basis of benthic community composition. We study the reefs of Moorea (French Polynesia) where, using benthic communities time series we back-calculate reef structural complexity. We were able to retrace two relevant episodes of habitat destruction: the Acanthaster planci outbreak of 2006-2009 and cyclone Oli of 2010.

Material and Methods

1. Study area

Moorea is a tropical volcanic island of volcanic origin, located in the Pacific Ocean between 17.4714° and 17.6058° South and 149.7522° and 149.9269°' West. The island is shaped as a triangle with a perimeter of 61 km and coastlines facing north, southwest and southeast (**Fig. 1**). The island is encircled by a coral reef, that is 500 to 700 m wide; the only exception to this pattern is the Northeast extremity where the lagoon width is limited to few tens of meters. Moorea is exposed to Northwest winds from January to March. Tides are semidiurnal with an amplitude of less than 0.3 m (Chazottes et al. 1995; Leichter et al. 2013). The swell direction is from southwest to northeast during the whole year.

The reefs of Moorea are threatened by several disturbances of biotic and abiotic origin (Adjeroud et al. 2018). The most devastating biotic disturbances were the 1979 and 2006 Acanthatster planci outbreak, which reduced coral cover from 50% to 10% (in 1979; Berumen and Pratchett 2006) and from 50% to less than 10% (in 2006; Lamy et al. 2016). Abiotic disturbances also impacted Moorea island, with main cyclones recorded in 1991 (Wasa) and 2010 (Oli). The impact of Wasa reduced the coral cover by 5% to over 20% across all the island. In contrast, coral cover was reduced to lower than 5% by Cyclone Oli (Lamy et al. 2016; Adjeroud et al. 2018) (**Fig. 2**).

2. Rugosity measures

In Moorea, a total of 57 photogrammetric transects were surveyed in end-of-2015 – beginning-of-2016, at three different sites: Tiahura (North Coast, 21 transects); Haapiti (Southwest coast, 20 transects) and Temae (Southeast coast, 16 transects) (**Fig. 1**). Each transect consisted of swaths of 20m length and 2m width and all transects were carried out in the outer reef, between 5 and 8m depth. Each transect was set up fixing on the bottom a 2m-long chain and, perpendicularly to it, a 20m-long metered tape. A diver swam ≈2m above the sea-bottom, maintaining the swimming speed as constant as possible and collecting images with a GoPro Hero camera pointed towards the sea-bottom. The camera was set to collect photos (12 megapixels) in time-lapse mode (2 pictures per second). For each transect, we collected approximately 200 photos with a forward overlap of ≈90%, with the diver swimming over the length of the entire transect four times to allow optimal side overlap. After the collection of the photos, the diver noted the depth of each extremity of the chain and metered tape to use them in the photogrammetric process as Ground Control Points (GCPs). In the case of an on-the-job self-calibration, the camera calibration is derived from image coordinates measured in the mapping photography and including the camera calibration parameters as unknowns in a self-calibrating bundle adjustment (Harwin et al. 2015).

The set of photos and the GCPs collected were then used as input to Agisoft Photoscan (www.agisoft.com), a photogrammetry software based on the Structure from Motion (SfM) method (Ullman 1979; Westoby et al. 2012). We used Agisoft to build the orthophotomosaic and the Digital Elevation Model (DEM) of each transect, with the same procedure explained by Storlazzi et al. (2016). Details of the photogrammetric process are shown in the **Annex S1**. Subsequently, we imported the DEM in ArcGIS v10.2 and calculated the reef rugosity by dividing the surface of the DEM area by the area of its planar projection (approximately $40m^2$) (**Fig. 3**). For the 57 transects, we estimated an average horizontal error of 0.1±0.06m and average vertical error of 0.04±0.04m, internal to the reconstructed model. Only the vertical error

had an influence on the estimation of rugosity, but given the range of the error, it was considered negligible.

3. Benthic community description and assessment

The orthophotomosaics were imported into Coral Point Count, which was used with an Excel extension v4.1 (Kohler and Gill 2006). We assessed the benthic cover placing 100 random points on the photomosaic and described 8 distinct benthic cover categories (**Table 1)**. A second dataset was used according to the CRIOBE surveys from 2004 to nowadays and consists of 25m point intercept transects data collected at 13 sites around the island across three habitats (fringing reef, back reef, outer reef) and using the same benthic categories (**Fig. 1**). This classification is based on the guideline of the monitoring program created by SO CORAIL (http://observatoire.criobe.pf/CRIOBEData/), the coral reef observation program of the French National Institute for Earth Sciences and Astronomy (INSU). These categories enabled us to back-calculate structural complexity on time series data from Moorea. For matching both datasets according to the habitat, only the outer reef was selected.

4. Statistical analysis

Our main goal was to calibrate a model that predicts structural complexity according to the benthic community composition. Since benthic community cover is expressed as percentages, we preferred not to use them as predictor variables as they are heavily correlated, and collinearity would have been high. We preferred to build a database that include the time series data and our photogrammetry transects without transforming the data to perform multivariate analysis. Thus, the Euclidean distance could be used to conduce a Principal Component Analyses (PCA). The first five orthogonal axes (accounted for more than 75% of the variance) were then extracted to be used as predictor variables in the model. A lasso generalized linear model has been conducted to predict coral reef structural complexity

according to the 5 PCA axes. A 10-Fold cross validation was done and a step AIC procedure defining the best model was applied. Because the 57 transects were measured at the same depth, those transects were pooled together rather to apply a mixed model due to the lack of the data, making us benefit from a solid robustness. The best model selected kept only 3 PCA dimensions. According to the k-fold analysis, k R^2 were obtained giving a necessary uncertainty for the model. This method appears more meaningful estimate than classical R^2 when the model has to be used for predictions. The lasso generalized linear model was then applied to time series data to back-calculate structural complexity and to test whether our model was able to detect drops of structural complexity due to the major perturbations.

The PCA data for the time series in Moorea were used to produce PCA plots and define the long-term tendencies in order to descriptively assess the entity of the effect of the Acanthaster planci outbreak (2006-2009) and the Oli cyclone (2010) on benthic communities. An ANOVA was then applied with the aim to define several bunches of similar years according to the PCA axes. To match those years with each other, a Tukey post-hoc analysis was conducted and a matrix of results was elaborated. Finally, special attention has been given about the Acropora spp. cover, Pocillopora spp. cover and rugosity index in 2004 (pre-disturbance year, with the high percent cover of corals) and 2017 (post-disturbance year, with the high percent cover of corals) to define a potential resilience or recovery (**Table S1**).

Results

The analysis of time series revealed that coral diversity was higher in 2004 with a percent cover of corals (CC) of 44.08% (**Fig. 4**). The CC decreased from 2004 to 2010 down to a minimum of 3.62%, which corresponds to the event of Cyclone Oli. After the cyclone passed, the coral cover increased over time until the end of the series (2017) with a final value of 42.77%. In 2004 the coral reefs of Moorea also showed a greater diversity of coral morphology (massive, branching in general, columns and encrusting). The assemblages

remained fairly stable despite a slow decline of the CC the first 2 years (CC_{2004} = 44.08% to CC_{2006} = 40.62%). Then, a first Crown-Of-Thorns Starfish (COTS) outbreak was reported in early 2006 (Kayal et al. 2012) and continued until 2009. The following year, cyclone Oli hit the island further decreasing the CC. After these events and until 2014, the substrate consisted of rubble and cobbles. From 2015, the CC recovered to a state similar to that of 2004. However, compared to 2004, the coral cover in 2017 was dominated by Pocillopora spp. (20.10 ± 6.78% in 2004 vs 26.61 ± 14.52% in 2017) instead of a more diverse assemblage with a high abundance of Acropora spp (9.76 ± 5.61% vs 2.53 ± 1.90% in 2017).

The cross-validated R^2 ($CV\text{-}R^2$) from our model reaches 0.81 ± 0.12. The 3 dimensions used were all significant and non-correlate (**Table 2, Fig S1**). The back calculation of structural complexity captured these major shifts in community structure. High structural complexity was observed in 2005 and 2006. All sites were then predicted to lose complexity corresponding to the timing of COTS outbreak models present patterns of decrease and increase in rugosity, matching with the biotic and abiotic changes like the COTS outbreak and the Cyclone Oli, as discussed above (**Fig. 5**). The model also exemplifies that the resilience of structural complexity differs among the thirteen reefs studied around Moorea island. In 2004, the highest values of structural complexity were measured respectively at Pihaena (North), Motu Ahi (East) and Haapiti (Northwest) (3.86, 3.51 and 2.92 respectively) while the lowest were recorded in Maatea (Southeast), Tiahura (North) and Aroa (North) (2.26, 2.07 and 1.81 respectively). After the disturbances in 2010, the higher values were defined in Taotaha (Northwest), Afareaitu (Southeast) and Entre 2 Baies (North) (2.08, 2.10 and 2.10 respectively) while the lowest values were documented at Haapiti (Northwest), Tiahura (North) and Maatea (Southeast) (1.84, 1.66 and 1.15 respectively). Finally, in 2017, the 3 lowest values were measured on the East coast (Motu Ahi, Maatea and Temae with rugosity values of 2.35, 2.12 and 1.98 respectively) while the sites located

on the northwest side (Entre 2 Baies, Tiahura and Gendron) presented the 3 higher rugosity scores (4.36, 4.31 and 3.53 respectively).

Finally, rugosity values rise to values equivalent to the first year of monitoring, during the last year of monitoring in 2017. The presence of Acropora spp. shows a significant difference between 2004 and 2017. However, no significant difference could be observed in either the Pocillopora spp. presence or the rugosity score (**Fig. 6**). In addition, the ANOVA followed by the post-hoc analysis confirmed a difference between two bunches of years according to the complexity around the island. Indeed, two profiles were highlighted: 1) one from 2004 to 2007 and 2016 to 2017 and 2) one from 2008 to 2015. These results support that the 3D complexity came back to an equilibrium four years after the Oli cyclone (**Table S1**).

Discussion

In this study we used a combination of methods – coral reef photogrammetry and statistical models – to test the potential to use species composition data to predict the structural complexity of coral reef assemblages. The use of the photogrammetry allowed us to obtain a three-dimensional metric of structural complexity, compared to linear metrics classically used such as the chain transect (Burns et al. 2015). Photogrammetry permits us to cover 40m^2 of the reef in one dive of about 90 minutes, whereas the chain method usually requires approximatively 15 minutes for a simple 20m transect. However, even if the pixel size of 1.73 × 1.73 µm - used for defining the complexity - is higher resolution than what is achieved using chain and tape, the results have to be interpreted with cautious. Indeed, a number of studies have shown photogrammetry to be error prone in a number of different ways. Lavy et al. (2015) and Figueira et al. (2015) both found that branching corals and other complex growth forms produce more error in photogrammetry-based estimates of complexity compared to in situ methods. Furthermore, Bryson et al. (2017) found that environmental conditions,

253 postprocessing, and even taking photos underwater can impact the accuracy of 3D structure
254 estimates using photogrammetry. In addition, this model is relevant for planar parts of the
255 reef, however, facing dropoff would be challenging. This technique requires swimming
256 over the bottom, nevertheless, as the more the distance you add between you and the
257 bottom, the worst the reconstruction will be. Finally, all the hidden part (not present in
258 the photos) are not reconstructed (e.g. what is inside a hole). The latter limit causes
259 relatively heavy consequences to define an accurate measure of the rugosity in those
260 conditions. From a statistical point of view, Carroll et al. (2006) defined 3 different regimes of
261 swell in Moorea which could altered the benthic composition, according to the exposure due to
262 the side of the island. Even if these affirmations are directly observable concerning the rugosity
263 in 2017 with our current model (lowest values on the east coast and higher values on the north
264 coast) a mixed model would have been more relevant. Unfortunately, only 16 transects were
265 done on the southeast side of Moorea which is not allowed us for using a mixed model. The
266 robustness of the model would have been directly impacted by the lack of residuals (rugosity
267 values sometimes lower than 1; Launer & Wilkinson, 2014). As per any statistical model, the
268 accuracy of prediction will increase with the size of the calibrating dataset. In that context, more
269 data will likely be needed to accurately capture spatial variation.
270 Despite these limits, we have found a significant relationship between reef structural
271 complexity and the composition of the benthic assemblages. Indeed 3 PCA axes were enough
272 to accurately predict complexity with a high accuracy (CV-R^2 = 0.81 ± 0.12). To validate our
273 model, we compared our values to (Kayal et al. 2017). These authors have found values at 12m-
274 depth of 1.44 ± 0.08, 1.41 ± 0.05 and 1.70 ± 0.03 for Haapiti, Tiahura and Entre 2 Baies
275 respectively. Our model suggests values for these locations of 1.75 ± 0.50, 1.68 ± 0.47 and 1.70
276 ± 0.60 respectively. Thus, even according the huge range of the uncertainties, our results
277 highlight the potential to use statistical modeling to predict structural complexity when this
278 information is lacking. Given the importance of structural complexity in ecological functioning

279 of coral reefs, the reconstruction of structural complexity is critical from long-term benthic
280 historical data, if we want to better understand and predict changes in coral reefs. For example,
281 Graham and Nash (2013) reviewed 20 studies using chain method to measure coral reef rugosity
282 in the Caribbean and found a strong negative relationship between structural complexity and
283 algal cover, a positive relationship between the structural complexity and the coral cover, and
284 a strong positive relationship between structural complexity and fish density and biomass.
285 Later, Graham et al. (2015) demonstrated that structural complexity is the main predictor of
286 coral reef recovery capacity after acute disturbance. This metric represents thus a key variable
287 of coral reef status, and apodictically exists also regarding the present day flattening of coral
288 reefs under the influence of climate change and human impacts. Back-calculating structural
289 complexity, with due caution, may be important to infer present coral reef status compared to
290 historical or quasi-pristine conditions.

291 Here, we have documented major changes in benthic assemblages across Moorea's coral
292 reefs (Berumen and Pratchett 2006; Adjeroud et al. 2018). Acropora spp. and Pocillopora spp.
293 were dominant species in 2003 (Berumen and Pratchett 2006) and this was still the case in 2004.
294 Pocillopora spp. then, Acropora spp. were affected by both COTS outbreak and the Oli cyclone
295 more than any other taxon (Kayal et al. 2012). Branching and table-shaped species belonging
296 to the genus Acropora were affected first and most heavily. Then, it was followed by those of
297 sub-branching Pocillopora. Finally, Populations of encrusting Montipora, massive Porites, and
298 other hard-coral assemblages also declined, showing a synchronized collapse with the entire
299 coral communities. From 2011 onward, benthic assemblages started to recover mainly thanks
300 to encrusting coral forms and Pocillopora spp. that is presently the dominating coral form in
301 Moorea. The current Pocillopora-dominated state may be a transitional phase, indicative of
302 either continuing degradation or recovery (Aronson et al. 2004). Our back-calculated structural
303 complexity was able to capture major changes due to COTS outbreak and Cyclone Oli, thus
304 attesting the potential to use statistical modeling when the rugosity has not been empirically

collected. However, the status of coral reefs in 2004 when Acropora spp. was on average ≈10% and the present status (average Acropora cover ≈2%) was not enough to distinguish difference in back-calculated structural complexity. There are two proposed explanations for this observation: (a) our model is calibrated with present-day data. Only two transects in 2017 had assemblages with an Acropora cover higher than 5% which is a consequent statistic assumption according to the Acropora cover in 2004 (9.76 ± 5.61% in 2004 vs 2.53 ± 1.90% in 2017). This again results in an extremely cautious interpretation of the results due to a possible underestimation of Acropora spp. in the past years (Aronson and Precht 2006; Alvarez-Filip et al. 2009, 2011). And/or (b) Acropora and Pocillopora taxa harbored branching form and similarly contribute to the complexity (Reichert et al. 2017). Thus, the complexity could be rebuilt according to the coral cover underlying the different coral morphologies (Halford et al. 2004; Graham and Nash 2013; Richardson et al. 2017). In order to sharp our hindcasting, the reproducibility of this method could allow us to find a new area with the needed information (i.e. past Acropora and Pocillopora cover vs post Acropora and Pocillopora cover and past and post rugosity) and to test our model. Waiting for this improvement, the CC could be enough accurate to rebuild the past and to predict the complexity for the coming years. Indeed, today more than ever, global coral reefs are witnessing the effects of climate changes, local impacts and natural stressors. Coral bleaching is affecting global coral reefs with an unprecedented frequency and intensity and the future structural complexity of coral reefs is expected to be reduced by these repeated perturbations (Hughes et al. 2018; Lough et al. 2018). As a consequence a loss of ecological diversity productivity is likely (Alvarez-Filip et al. 2009).

Conflict of interest: On behalf of all authors, the corresponding author states that there is no conflict of interest.

References

Adjeroud M, Vercelloni J, Bosserelle P, Chancerelle Y, Kayal M, Iborra-Cantonnet C, Penin L, Liao V, Claudet J (2018) Recovery of coral assemblages despite acute and recurrent disturbances on a South Central Pacific reef. Sci Rep 8:8

Alvarez-Filip L, Côté IM, Gill JA, Watkinson AR, Dulvy NK (2011) Region-wide temporal and spatial variation in Caribbean reef architecture: Is coral cover the whole story? Glob Chang Biol 17:2470–2477

Alvarez-Filip L, Dulvy NK, Gill JA, Côté IM, Watkinson AR (2009) Flattening of Caribbean coral reefs: Region-wide declines in architectural complexity. Proc R Soc B Biol Sci 276:3019–3025

Aronson RB, MacIntyre IG, Wapnick CM, O'Neill MW (2004) Phase shifts alternative states and the unprecedented convergence of two reef systems. Ecol Soc Am 85:1876–1891

Aronson RB, Precht WF (2006) Conservation, precaution, and Caribbean reefs. Coral Reefs 25:441–450

Berumen ML, Pratchett MS (2006) Recovery without resilience: Persistent disturbance and long-term shifts in the structure of fish and coral communities at Tiahura Reef, Moorea. Coral Reefs 25:647–653

Bryson M, Ferrari R, Figueira W, Pizarro O, Madin J, Williams S, Byrne M (2017) Characterization of measurement errors using structure-motion and photogrammetry to measure marine habitat structural complexity. Ecol Evol 7:5669–5681

Burns J, Delparte D, Gates R, Takabayashi M (2015) Integrating structure-from-motion photogrammetry with geospatial software as a novel technique for quantifying 3D ecological characteristics of coral reefs. PeerJ 3:19

Carroll A, Harrison P, Adjeroud M (2006) Sexual reproduction of Acropora reef corals at Moorea , French Polynesia. Coral Reefs 25:93–97

Casella E, Collin A, Harris D, Ferse S, Bejarano S, Parravicini V, Hench JL, Rovere A (2017) Mapping coral reefs using consumer-grade drones and structure from motion photogrammetry techniques. Coral Reefs 36:269–275

Chazdon RL (2014) Second Growth, the promise of tropical forest regeneration in an age of deforestation.

Chazottes V, Le Campion-Alsumard T, Peyrot-Clausade M (1995) Bioerosion rates on coral reefs : interactions between macroborers , * Experimental site. Palaeogeogr Palaeoclimatol Palaeoecol 113:189–198

Figueira W, Ferrari R, Weatherby E, Porter A, Hawes S, Byrne M (2015) Accuracy and Precision of Habitat Structural Complexity Metrics Derived from Underwater Photogrammetry. Remote Sens 7:16883–16900

Friedman A, Pizarro O, Williams SB, Johnson-Roberson M (2012) Multi-Scale Measures of Rugosity, Slope and Aspect from Benthic Stereo Image Reconstructions. PLoS One 7:14

Graham NAJ, Jennings S, MacNeil MA, Mouillot D, Wilson SK (2015) Predicting climate-driven regime shifts versus rebound potential in coral reefs. Nature 518:7

Graham NAJ, Nash KL (2013) The importance of structural complexity in coral reef ecosystems. Coral Reefs 32:315–326

Gratwicke B, Speight MR (2005) Effects of habitat complexity on Caribbean marine fish assemblages. Mar Ecol Prog Ser 292:301–310

Halford A, Cheal AJ, Ryan D, Williams DM (2004) Resilience to Large-Scale Disturbance in Coral and Fish Assemblages on the Great Barrier Reef. Ecol Soc Am 85:1892–1905

Harris DL, Pomeroy A, Power H, Casella E, Rovere A, Webster JM, Parravicini V, Canavesio R, Collin A (2018) Coral reef structural complexity provides important coastal protection from waves under rising sea levels. Sci Adv 4:7

Harwin S, Lucieer A, Osborn J (2015) The Impact of the Calibration Method on the Accuracy of Point Clouds Derived Using Unmanned Aerial Vehicle Multi-View Stereopsis. Remote

387 Sens 7:11933–11953
388 Heron SF, Maynard JA, Van Hooidonk R, Eakin CM (2016) Warming Trends and Bleaching
389 Stress of the World's Coral Reefs 1985-2012. Sci Rep 6:14
390 Hill J, Wilkinson C (2004) Methods for ecological monitoring of coral reefs: A resource for
391 managers. Version 1. Australian Institute of Marine Science, Townsville, 117.
392 Hobson RD (1972) Surface Roughness in Topography: A Quantitative Approach. Spatial
393 Analysis in Geomorphology 221-245
394 Hoegh-Guldberg O (1999) Climate Change, coral bleaching and the future of the world' s coral
395 reefs. Mar Freshw Res 50:839–866
396 Hoegh-Guldberg O, Mumby PJ, Hooten AJ, Steneck RS, Greenfield P, Gomez E, Harvell CD,
397 Sale PF, Edwards AJ, Caldeira K, Knowlton N, Eakin CM, Iglesias-Prieto R, Muthiga N,
398 Bradbury RH, Dubi A, Hatziolos ME (2007) Coral reefs under rapid climate change and
399 ocean acidification. Science (80-) 318:1737–1742
400 Hughes TP, Álvarez-Noriega M, Álvarez-Nomero JG, Anderson KD, Baird AH, Babcock RC,
401 Beger M, Bellwood DR, Berkelmans R, Bridge TC, Butler IR, Byrne M, Cantin NE,
402 Comeau S, Connolly SR, Cumming GS, Dalton SJ, Kerry JT, Kuo C, Lough JM, Hoey
403 AS, Hobbs JA, Hoogenboom MO, Emma V, Pears RJ, Pratchett MS, Schoepf V, Simpson
404 T, Skirving WJ, Sommer B (2017) Global warming and recurrent mass bleaching of corals.
405 Nature 543:373–377
406 Hughes TP, Anderson KD, Connolly SR, Heron SF, Kerry JT, Lough JM, Baird AH, Baum JK,
407 Berumen ML, Bridge TC, Claar DC, Eakin CM, Gilmour JP, Graham NAJ, Harrison H,
408 Hobbs JA, Hoey AS, Hoogenboom M, Lowe RJ, Mcculloch MT, Pandolfi JM, Pratchett
409 M, Schoepf V (2018) Spatial and temporal patterns of mass bleaching of corals in the
410 Anthropocene. Science (80-) 83:80–83
411 Hughes TP, Baird AH, Bellwood DR, Card M, Connolly SR, Folke C, Grosberg R, O. H-G,
412 Jackson JBC, Kleypas J, Lough JM, Marshall P, Nyström M, Palumbi SR, Pandolfi JM,
413 Rosen B, Roughgarden J (2003) Climate Change, Human Impacts, and the Resilience of
414 Coral Reefs. Science (80-) 301:929–933
415 Kayal M, Bosserelle P, Adjeroud M (2017) Bias associated with the detectability of the coral-
416 eating pest crown-of-thorns seastar and implications for reef management Subject
417 Category : Subject Areas : R Soc Open Sci 4(8), 170396.
418 Kayal M, Vercelloni J, Lison de Loma T, Bosserelle P, Chancerelle Y, Geoffroy S, Stievenart
419 C, Michonneau F, Penin L, Planes S, Adjeroud M (2012) Predator Crown-of-Thorns
420 Starfish (Acanthaster planci) Outbreak, Mass Mortality of Corals, and Cascading Effects
421 on Reef Fish and Benthic Communities. PLoS One 7(10), e47363.
422 Kohler KE, Gill SM (2006) Coral Point Count with Excel extensions (CPCe): A Visual Basic
423 program for the determination of coral and substrate coverage using random point count
424 methodology. Comput Geosci 32:1259–1269
425 Lamy T, Galzin R, Kulbicki M, Lison de Loma T, Claudet J (2016) Three decades of recurrent
426 declines and recoveries in corals belie ongoing change in fish assemblages. Coral Reefs
427 35:293–302
428 Launer RL, & Wilkinson GN (2014) Robustness in statistics. Academic Press.
429 Lavy A, Eyal G, Neal B, Keren R, Loya Y, Ilan M (2015) A quick , easy and non-intrusive
430 method for underwater volume and surface area evaluation of benthic organisms by 3D
431 computer modelling. Methods Ecol Evol 6:521–531
432 Leichter JJ, Alldredge AL, Bernardi G, Brooks AJ, Carlson CA, Carpenter RC, Edmunds J,
433 Fewings, M. R, Hanson, K. M, Hench, J. L, Holbrook J, Nelson, G. E, Schmitt, R. J,
434 Toonen, R. J, Washburn L, Wyatt, S. J (2013) Biological and physical interactons on a
435 tropical island coral reef: transport, and retention processes on Moorea, French Polynesia.
436 Oceanography 26:52–63
437 Leon JX, Roelfsema CM, Saunders MI, Phinn SR (2015) Measuring coral reef terrain
438 roughness using "Structure-from-Motion" close-range photogrammetry. Geomorphology

242:21–28
Lough JM, Anderson KD, Hughes TP (2018) Increasing thermal stress for tropical coral reefs : 1871 – 2017. Sci Rep 1–8
MacArthur RH, Wilson EO (1967) The Theory of Island Biogeography.
McCormick MI (1994) Comparison of field methods for measuring surface tomography and their associations with a tropical reef fish assemblage. Mar Ecol Prog Ser 112:87–96
Naughton P, Kastner R, Sandin S, Kuester F, Edwards C, Petrovic V (2015) Scaling the Annotation of Subtidal Marine Habitats. Proc 10th Int Conf Underw Networks Syst 1–5
Newman SP, Meesters EH, Dryden CS, Williams SM, Sanchez C, Mumby PJ, Polunin NVC (2015) Reef flattening effects on total richness and species responses in the Caribbean. J Anim Ecol 84:1678–1689
Van Oppen MJH, Lough JM (2009) Coral Bleaching Patterns, Processes, Causes and Consequences.
Parravicini V, Rovere A, Donato M, Morri C, Bianchi CN (2006) A method to measure three-dimensional substratum rugosity for ecological studies: an example from the date-mussel fishery desertification in the north-western Mediterranean. J Mar Biol Assoc United Kingdom 86:689–690
Perry CT, Alvarez-Filip L, Graham NAJ, Mumby PJ, Wilson SK, Kench PS, Manzello DP, Morgan KM, Slangen ABA, Thomson DP, Januchowski-Hartley F, Smithers SG, Steneck RS, Carlton R, Edinger EN, Enochs IC, Estrada-Saldívar N, Haywood MDE, Kolodziej G, Murphy GN, Pérez-Cervantes E, Suchley A, Valentino L, Boenish R, Wilson M, Macdonald C (2018) Loss of coral reef growth capacity to track future increases in sea level. Nature 558:396–400
Reichert J, Backes AR, Schubert P, & Wilke T (2017) The power of 3D fractal dimensions for comparative shape and structural complexity analyses of irregularly shaped organisms. Methods in Ecology and Evolution, 8(12), 1650-1658.
Richardson LE, Graham NAJ, Hoey AS (2017) Cross-scale habitat structure driven by coral species composition on tropical reefs. Sci Rep 7:11
Risk MJ (1972) Fish diversity on a coral reef in the virgin islands. Atoll Res Bull
Rogers A, Blanchard JL, Mumby PJ (2014) Vulnerability of coral reef fisheries to a loss of structural complexity. Curr Biol 24:1000–1005
Storlazzi CD, Dartnell P, Hatcher GA, Gibbs AE (2016) End of the chain? Rugosity and fine-scale bathymetry from existing underwater digital imagery using structure-from-motion (SfM) technology. Coral Reefs 35:889–894
Ullman S (1979) The interpretation of structure from motion. Proc R Soc Lond B Biol Sci 203:405–426
Westoby MJ, Brasington J, Glasser NF, Hambrey MJ, Reynolds JM (2012) "Structure-from-Motion" photogrammetry: A low-cost, effective tool for geoscience applications. Geomorphology 179:300–314
Willis TJ, Anderson MJ (2003) Structure of cryptic reef fish assemblages: relationships with habitat characteristics and predator density. Mar Ecol Prog Ser 257:209–221

Figures

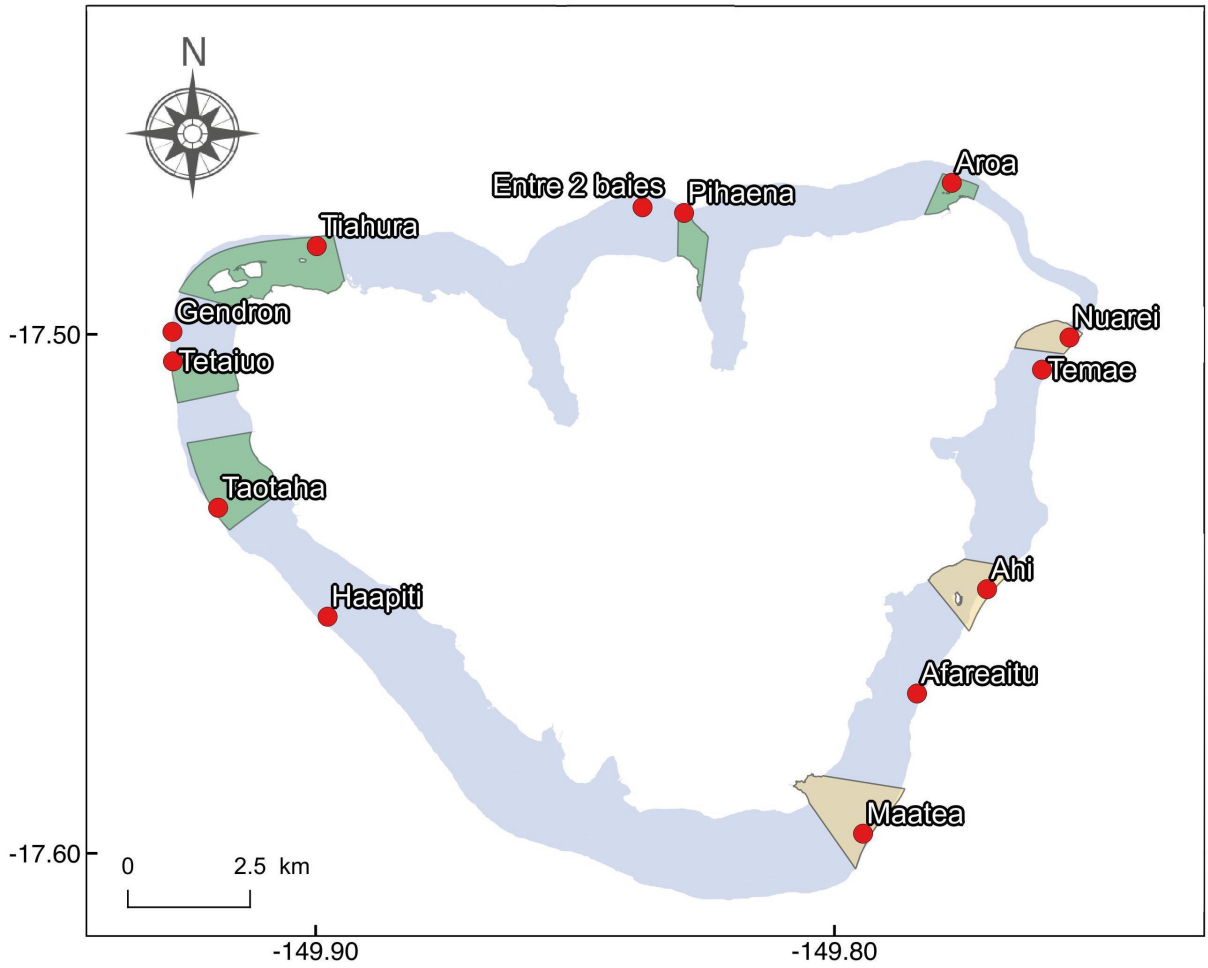

Fig. 1 Location of the 13 sites sampled each year since 2004 from 2017 of the MPA monitoring (red dots) around the island of Moorea. The 5 fully protected MPAs are highlighted in green and the restricted MPAs are highlighted in yellow. The 5 sites outside of the MPAs are controls.

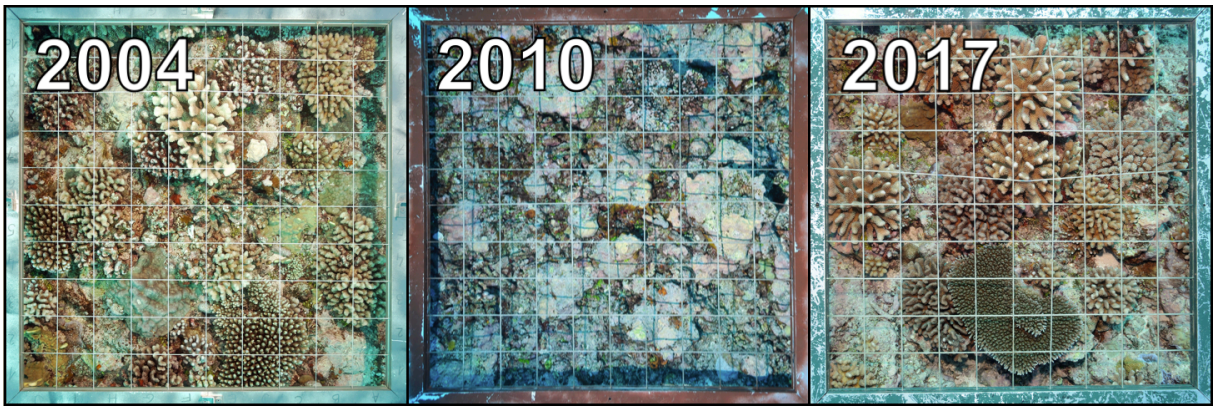

Fig. 2 Evolution of one of the twenty quadrats used to define the coral cover in Haapiti (South West of the island) before (in 2004), during (in 2010) and after (in 2017) Cyclone Oli.

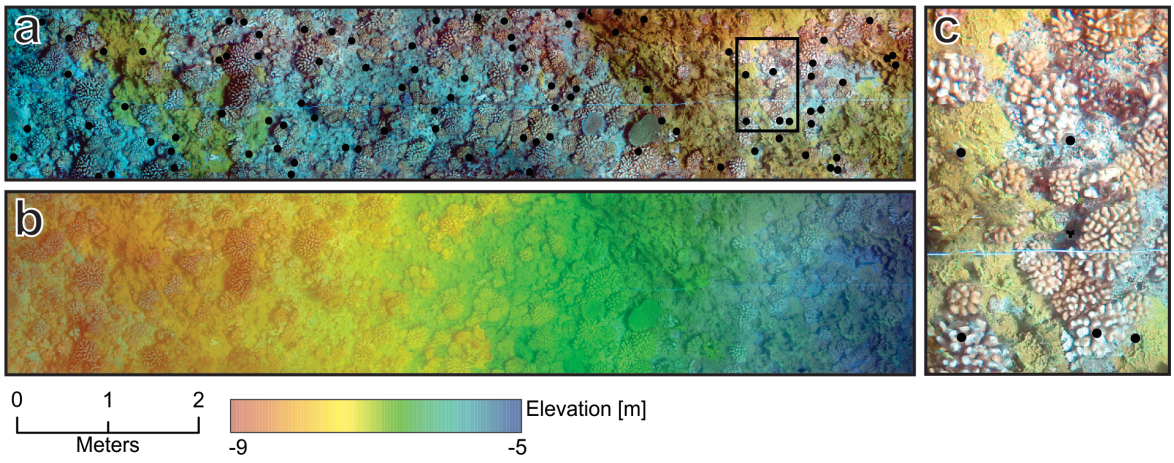

Fig. 3 Example of results from underwater photogrammetry. a) Orthorectified photomosaic. The black dots indicate the random points where the shape classification has been carried out. b) Digital Elevation Model representing depth values (the photomosaic is kept in transparency in the background). c) Detail of the photomosaic.

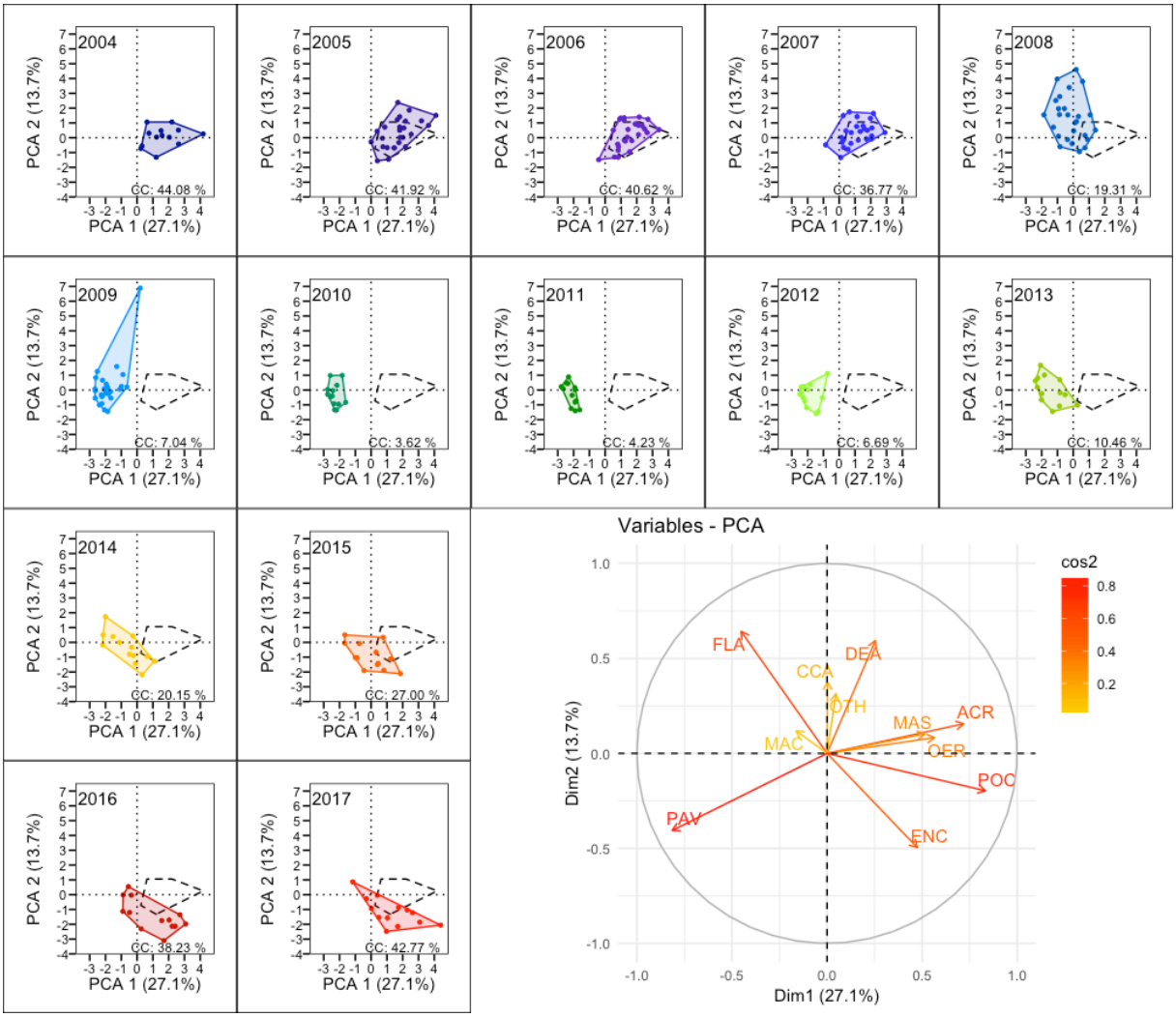

Fig. 4 Principal Components Analysis (PCA) using the 11 morpho-species respecting the code as follows: ACR - Acropora spp; CCA - Crustose Coralline Algae; DEA - Dead Coral; ENC - Encrusting Corals; FLA - Flat (Sand or Mud); MAC - Macroalgae; MAS - Massive corals; OER

- Other Erects Forms; OTH - Others (Sponges or benthic species); PAV - Pavement; and POC - Pocillopora spp. The PCA was used year by year from 2004 to 2017 and the coral cover (CC) is written at the bottom right of each box. The coral community in 2004 is referred as model in black dashed lines each year.

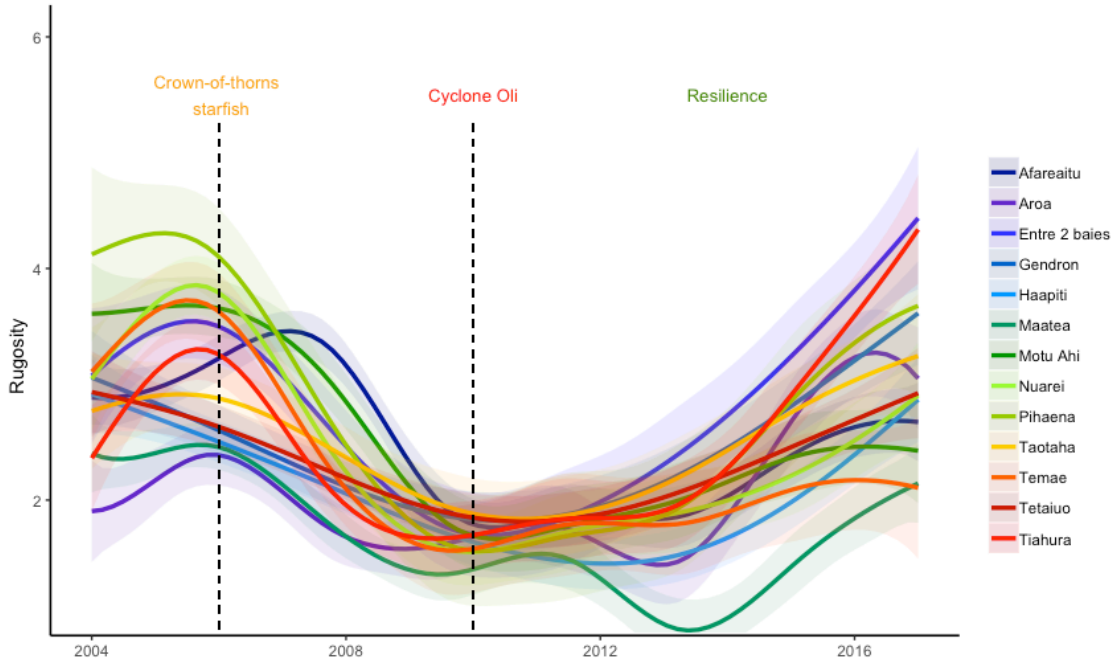

Fig. 5 Rugosity reconstruction from 2004 to 2017 according to the average model and according to the 13 sites around the island of Moorea. Both biologic invasion and extreme climatic weather events are shown for respectively 2006 and 2010.

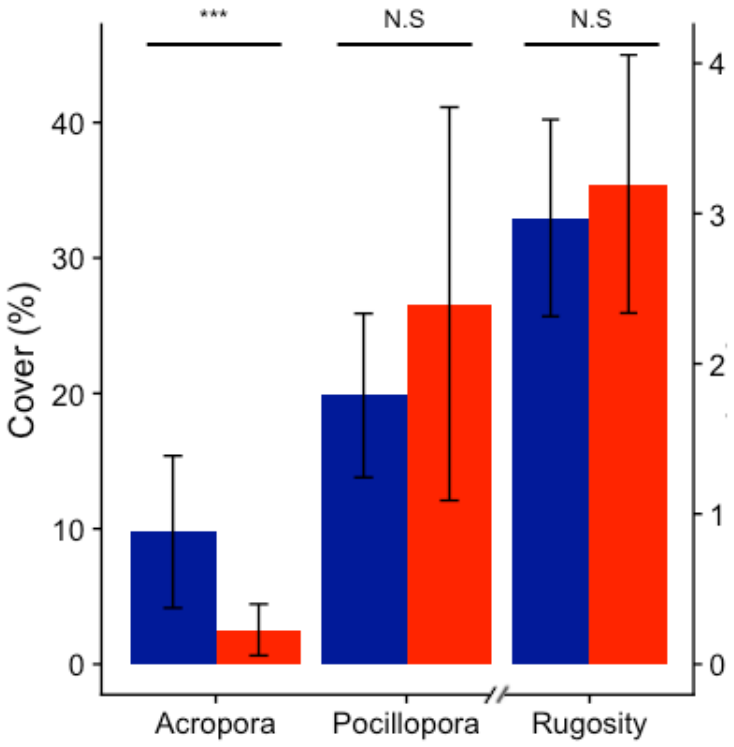

Fig. 6 Difference between the Acropora and the Pocillopora cover (%) on the left, and the difference in rugosity (index) on the right. The dark blue color represents 2004 instead of 2017 is representing in red. The p-value is represented on the top of each barplot according to the

significant R code (*** highly significant (<0.001), **very significant (<0.01), * significant (<0.05), . almost significant (<0.1), N.S non-significant; threshold: p-value = 0.05)

Tab. 1 Categories of shape classification defined and used to rebuild the rugosity these last 14 years. 9 variables are morphologic instead a distinction at the genus level is done for Acropora spp. and Pocillopora spp. The CCA was differentiated from the pavement according to their extension: when this later was higher than 100 cm^2, which corresponds to a projected surface of a circle of radius of 5-6 cm it was considered as CCA rather than pavement. The dead corals category understands rubbles and cobbles. The flattening category represents sand or mud substrate. The categories Encrusting, Other Erect Forms and Massive represent different coral morphologies. Finally, the others category represents mostly benthic organism like echinoid or even sponges.

ACR	Acropora spp.
CCA	Coralline Crustose Algae
DEA	Dead corals
ENC	Encrusting corals
FLA	Flat (Mud, Sand)
MAC	Macroalgae
MAS	Massive corals
OER	Corals with other erects forms
OTH	Other (like echinoid)
PAV	Pavement
POC	Pocillopora spp.

Tab. 2 Coefficients and standard error for each parameter according to best model defined: **Rugosity ~ Dim 1 + Dim 3 + Dim 5** (AIC = 71.776 and R^2 = 0.81 ± 0.12). The p-value represents the significance of each parameters according to the R code (*** highly significant (<0.001), **very significant (<0.01), * significant (<0.05), . almost significant (<0.1), N.S non-significant; threshold: p-value = 0.05)

	Estimate	Standard Error	p-value
Intercept	1.65970	0.14616	1.08e-15 (***)
Dimension 1	0.53283	0.08602	9.48e-08 (***)
Dimension 3	0.41917	0.07003	2.03e-07 (***)
Dimension 5	-0.15003	0.06090	1.71e-02 (*)

Appendix

Tab. S1 Post Hoc (Tukey HSD) matrix for testing the rugosity difference according to each year combination. The P-value (threshold: 0.05) for each combination is written in the matrix data as follows. The red values are significantly differents and the blue values are not.

	2004	**2005**	**2006**	**2007**	**2008**	**2009**	**2010**	**2011**	**2012**	**2013**	**2014**	**2015**	**2016**	**2017**
2004	1,00													
2005	0.98	1.00												
2006	0.96	1.00	1.00											
2007	1.00	0.87	0.80	1.00										
2008	0.04	0.00	0.00	0.00	1.00									
2009	0.00	0.00	0.00	0.00	0.93	1.00								
2010	0.00	0.00	0.00	0.00	0.96	1.00	1.00							
2011	0.00	0.00	0.00	0.00	0.95	1.00	1.00	1.00						
2012	0.00	0.00	0.00	0.00	0.98	1.00	1.00	1.00	1.00					
2013	0.01	0.00	0.00	0.00	1.00	1.00	1.00	1.00	1.00	1.00				
2014	0.11	0.00	0.00	0.03	1.00	1.00	0.99	0.99	1.00	1.00	1.00			
2015	0.91	0.05	0.04	0.81	1.00	0.20	0.31	0.30	0.35	0.51	0.98	1.00		
2016	1.00	1.00	0.99	1.00	0.01	0.00	0.00	0.00	0.00	0.00	0.05	0.80	1.00	
2017	1.00	1.00	1.00	1.00	0.00	0.00	0.00	0.00	0.00	0.00	0.00	0.34	1.00	1.00

Fig. S1 Analysis of the residuals (fitted values vs observations) from the total model: Rugosity ~ Dim 1 + Dim 2 + Dim 3 + Dim 4 + Dim 5 (AIC = 71.8, $R^2 = 0.78 \pm 0.08$) on the left and the best model Rugosity ~ Dim 1 + Dim 3 + Dim 5 (AIC = 73.6, $R^2 = 0.81 \pm 0.12$) on the right.

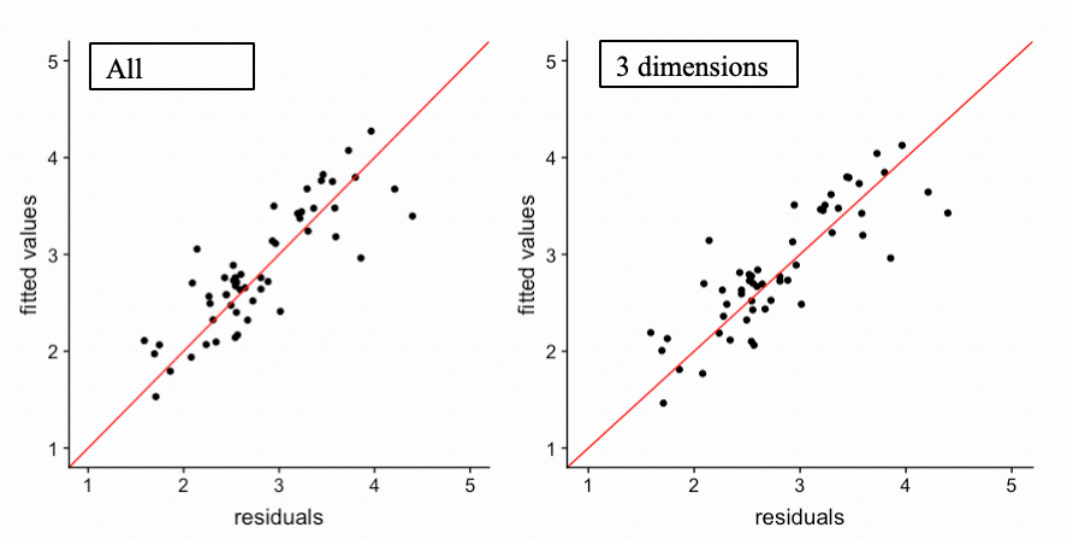

Annex

Annex S1 Report from Agisoft Photoscan for one site, detailing the settings used for the processing of underwater photos.

1. **Survey Data**

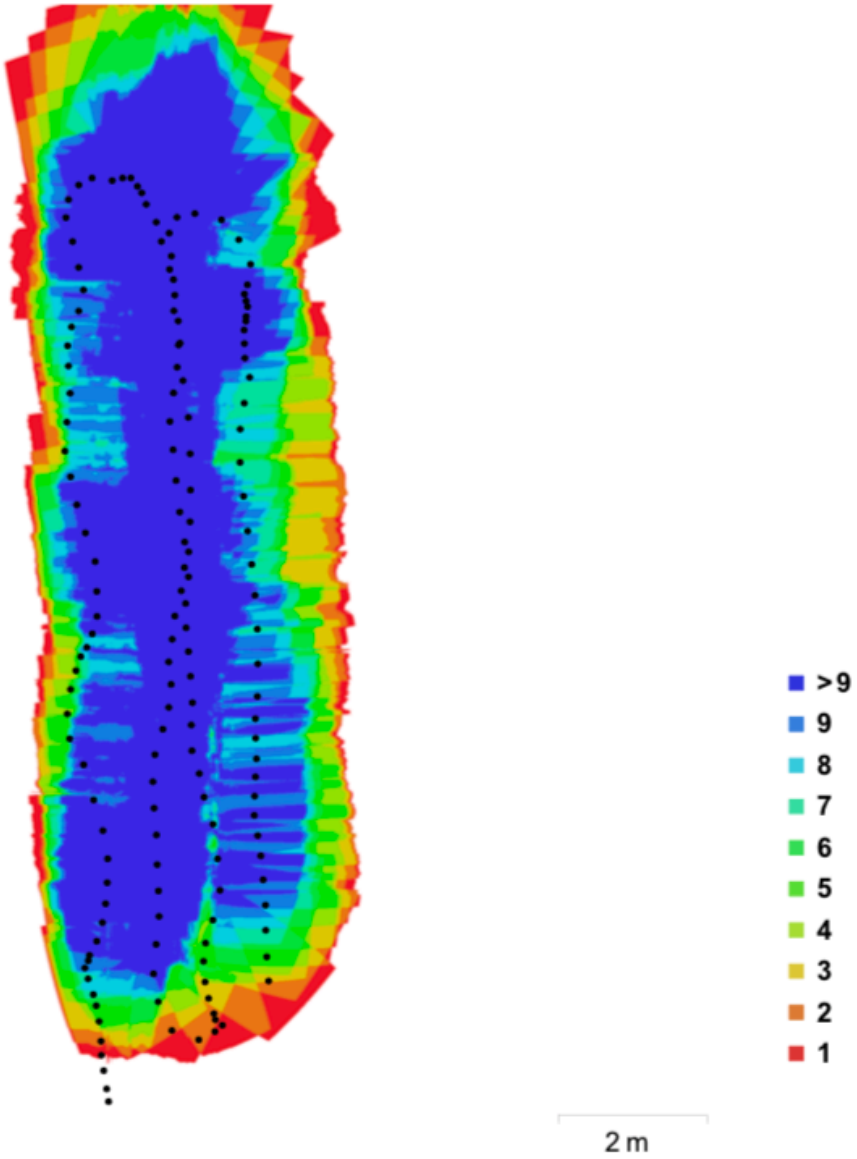

Fig. 1 Camera locations and image overlap

Number of images:	157	Camera stations:	157
Flying attitude:	2.56m	Tie points:	139.838
Ground resolution:	0.53 mm/pix	Projections:	383.598
Coverage area:	56.3 sq m	Reprojection error:	1.88 pix

Tab. 1 Cameras

Camera Model	Resolution	Focal Length	Pixel Size
HERO4 Black (3 mm)	4000 x 3000	3mm	1.73 x 1.73 um

2. **Camera calibration**

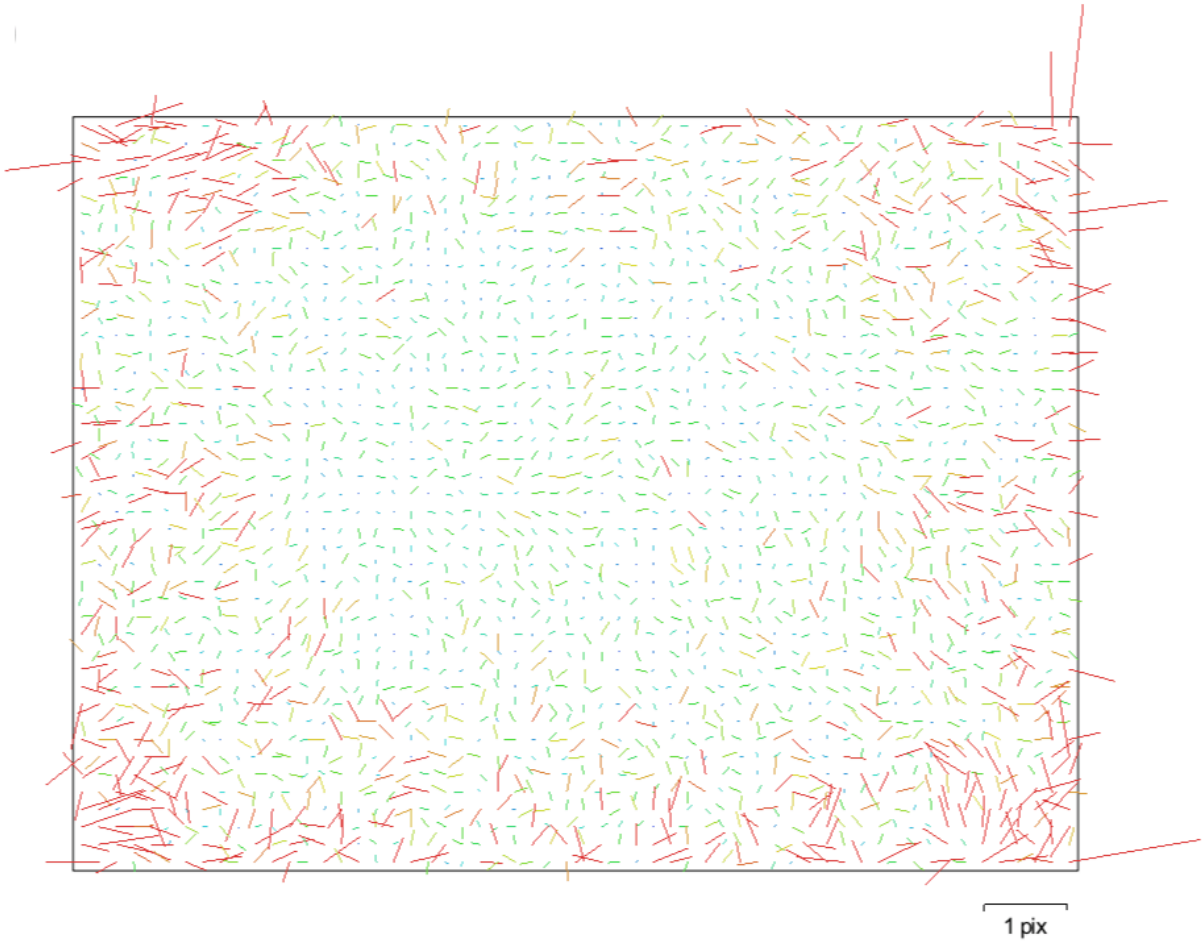

Fig. 2 Image residuals for HERO4 Black (3 mm).

HERO4 Black (3mm)
157 images

Resolution	Focal length	Pixel size	Precalibrated
4000x3000	**3 mm**	**1.73 x 1.73 µm**	**No**

Type:	Frame	Skew:	0
Fx:	4666.42	Cx:	2005.25
Fy:	4666.42	Cy:	1486.48
K1:	0.223613	P1:	0.00194777
K2:	0.373779	P2:	-0.00200162
K3:	1.24196	P3:	0
K4:	0	P4:	0

3. Ground Control Points

Fig. 3 GCP locations

Tab. 2 Control points

Label	XY error(m)	Z error (m)	Error (m)	Projections	Error (pix)
point1	0.206298	-0.0677987	0.217153	13	1.992
point2	0.0963633	0.0426041	0.105361	16	1.153
point3	0.039409	3.96756e-05	0.039409	17	0.051
point4	0.205045	0.0251539	0.206582	9	0.044
Total	**0.154468**	**0.0419657**	**0.160067**		**1.151**

4. Digital Elevation Model

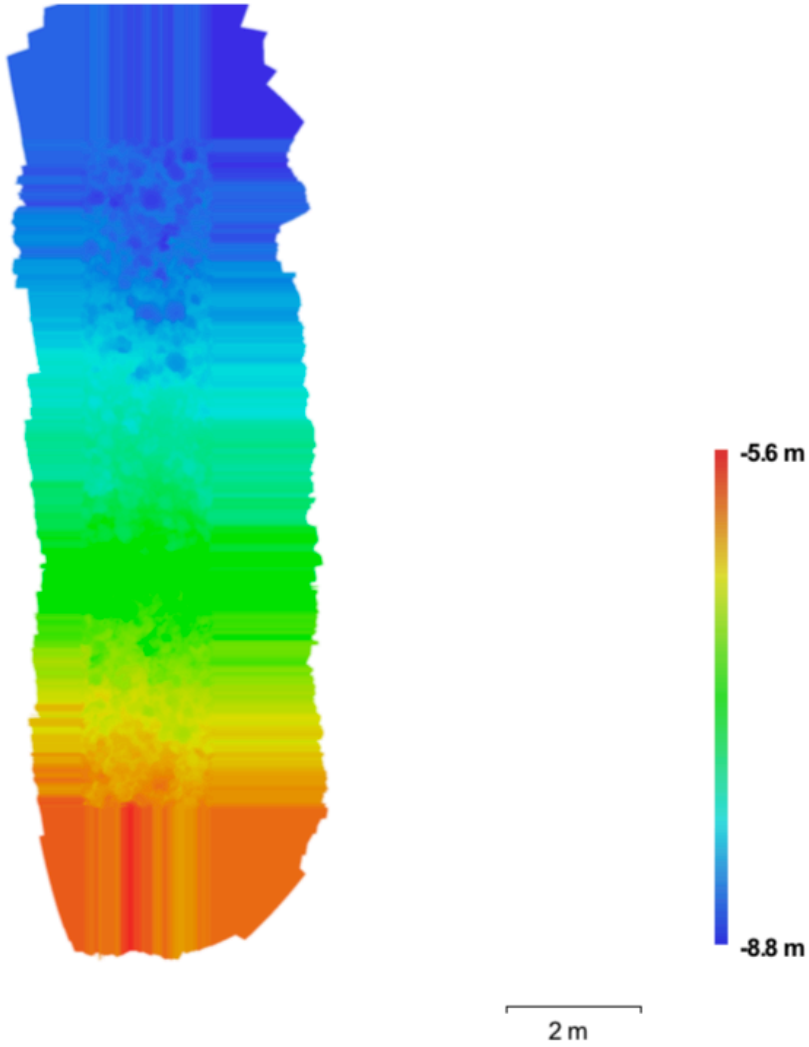

Fig. 4 Reconstructed digital elevation model.

Resolution: 1.06 mm/pix
Point density: 889956 points per sq m

5. Processing parameters

General	
Cameras	157
Aligned cameras	157
Markers	4
Coordinate system	Local Coordinates
Point Cloud	
Points	139,838 of 221,231
RMS reprojection error	0.382302 (1.88392 pix)
Max reprojection error	6.30304 (30.1948 pix)
Mean key point size	5.32459 pix
Effective overlap	2.94411
Alignment parameters	
Accuracy	High
Pair preselection	Disabled
Key point limit	40,000
Tie point limit	4,000
Constrain features by mask	No
Matching time	17 minutes 46 seconds
Alignment time	3 minutes 10 seconds
Optimization parameters	
Parameters	f, cx, cy, k1-k3, p1, p2
Optimization time	5 seconds
Dense Point Cloud	
Points	72,229,238
Reconstruction parameters	
Quality	High
Depth filtering	Aggressive
Processing time	8 minutes 29 seconds
Model	
Faces	4,815,282
Vertices	2,417,898
Reconstruction parameters	
Surface type	Arbitrary
Source data	Dense
Interpolation	Enabled
Quality	High
Depth filtering	Aggressive
Face count	4,815,282
Processing time	4 hours 29 minutes
DEM	
Size	1,886 x 9,433
Coordinate system	Local Coordinates
Reconstruction parameters	
Source data	Dense cloud
Interpolation	Enabled
Orthomosaic	
Size	3,773 x 18,867
Coordinate system	Local Coordinates
Channels	3, unit8
Blending mode	Mosaic
Reconstruction parameters	
Surface	Mesh
Enable color correction	No